A&A 446, 185–200 (2006)
DOI: 10.1051/0004-6361:20053293

Astronomy & Astrophysics

Diffractive interstellar scintillation of the quasar J1819+3845 at λ21 cm⋆

J.-P. Macquart[1,2,⋆⋆] and A. G. de Bruyn[3,1]

[1] Kapteyn Astronomical Institute, University of Groningen, PO Box 800, Groningen 9700 AV, The Netherlands
[2] National Radio Astronomy Observatory, PO Box 0, Socorro NM 87801, USA
e-mail: jmacquar@nrao.edu
[3] Netherlands Foundation for Research in Astronomy, Dwingeloo, The Netherlands
e-mail: ger@astron.nl

Received 25 April 2005 / Accepted 12 September 2005

ABSTRACT

We report the discovery of fast, frequency-dependent intensity variations from the scintillating intra-day variable quasar J1819+3845 at λ 21 cm which resemble diffractive interstellar scintillations observed in pulsars. The observations were taken with the Westerbork Synthesis Radio Telescope on a dozen occasions in the period between Aug. 2002 and Jan. 2005. The data were sampled at both high temporal and high frequency resolution and have an overall simultaneous frequency span of up to 600 MHz. In constructing the light curves and dynamic spectra the confusion from background sources has been eliminated. The timescale (down to 20 min) and the bandwidth (frequency decorrelation bandwidth of 160 MHz) of the observed variations jointly imply that the component of the source exhibiting this scintillation must possess a brightness temperature well in excess of the inverse Compton limit. A specific model in which both the source and scintillation pattern are isotropic implies a brightness temperature $0.5 \times 10^{13} z_{\rm pc}$ K, where previous estimates place the distance to the scattering medium in the range $z_{\rm pc} = 4{-}12$ pc, yielding a minimum brightness temperature >20 times the inverse Compton limit. An independent estimate of the screen distance using the 21 cm scintillation properties alone indicates a minimum screen distance of $z \approx 40$ pc and a brightness temperature above 2×10^{14} K. There is no evidence for anisotropy in the scattering medium or source from the scintillation characteristics, but these estimates may be reduced by a factor comparable to the axial ratio if the source is indeed elongated. The observed scintillation properties of J1819+3845 at 21 cm are compared with those at 6 cm, where a significantly larger source size has been deduced for the bulk of the emission by Dennett-Thorpe & de Bruyn (2003). However, opacity effects within the source and the different angular scales probed in the regimes of weak and strong scattering complicate this comparison.

Key words. galaxies: quasars: individual: J1819+3845 – galaxies: active – scattering – radiation mechanisms: non-thermal – techniques: high angular resolution

1. Introduction

The presence of intra-day variability (IDV) in some active galactic nuclei (AGN) at centimetre wavelengths (Heeschen 1984; Witzel et al. 1986) raises concern that the brightness temperatures of radio sources may violate the inverse Compton limit by several orders of magnitude (Quirrenbach et al. 1991; Kedziora-Chudczer et al. 1997).

It is now recognized that the variability is largely, if not exclusively, due to scintillation in the interstellar medium of our Galaxy (e.g. Jauncey et al. 2000; Lovell et al. 2003). This is established unequivocally for the IDV quasar J1819+3845. A ∼90 s time delay in the arrival times of the source's intensity variations measured between two widely-separated telescopes firmly identifies its variability with interstellar scintillation. The finite delay is attributed to the finite speed with which the scintillation pattern moves transverse to the line of sight (Dennett-Thorpe & de Bruyn 2002). An annual modulation in the timescale of the variability is also observed in J1819+3845, and is explained by the annual modulation in the scintillation velocity, $\boldsymbol{v}_{\rm ISS}$, due to the Earth's changing orbital velocity relative to the interstellar scattering material (Dennett-Thorpe & de Bruyn 2003). This annual cycle arises because the Earth's velocity is comparable to the velocity of the scattering material in the interstellar medium responsible for the intensity fluctuations. Annual cycles are also reported in several other IDV sources (Bignall et al. 2003; Rickett et al. 2001; Jauncey & Macquart 2001).

⋆ Appendix is only available in electronic form at http://www.edpsciences.org
⋆⋆ Jansky Fellow.

The brightness temperatures of IDV sources have proven difficult to constrain, largely because of the difficulty of determining the distance to the scattering material, z, responsible for the intensity fluctuations. These brightness temperatures have hitherto been estimated on the basis of the measurements made at $\lambda 6$ cm, at which flux variations are caused by weak interstellar scintillation. In this regime one measures the source variability timescale relative to the Fresnel timescale, $t_{\rm F} = r_{\rm F}/v_{\rm ISS} = (\lambda z/2\pi)^{1/2}/v_{\rm ISS}$ and thus deduces the source size relative to the angular scale subtended by the Fresnel scale, $\theta_{\rm F} = r_{\rm F}/z$. Despite these difficulties, several sources still exceed the inverse Compton limit by a large margin. A thorough analysis estimates the redshift-corrected brightness temperature of PKS 0405−385 at 5×10^{13} K (Rickett et al. 2002). A similar but less robust limit of $T_{\rm b} \geq 5\times10^{13}$ K is also derived for the source PKS 1519−273 (Macquart et al. 2000).

J1819+385 is estimated to possess a modest brightness temperature of approximately $\sim10^{12}$ K at 4.9 GHz (Dennett-Thorpe & de Bruyn 2003). The flux density of the source varies on timescales as short as 40 minutes at this frequency. These variations are also interpreted in terms of scintillation in the regime of weak scattering (Dennett-Thorpe & de Bruyn 2000). The estimated screen distance is small, in the range $z = 4-12$ pc, and the source is relatively weak, which accounts for the small brightness temperature despite its extremely rapid variability (Dennett-Thorpe & de Bruyn 2003).

This source generally exhibits slower variations at lower frequencies (Dennett-Thorpe & de Bruyn 2000). The dominant variations at 2.4 and 1.4 GHz occur on ∼6-h timescales during the same interval in the annual cycle of J1819+3845 in which dramatic intra-hour variations are observed at 4.9 GHz. Such a change in the character of the variability with decreasing frequency is typical of intra-day variable sources (Kedziora-Chudczer et al. 1997; Macquart et al. 2000; Quirrenbach et al. 2000). These slow variations are attributed to the increase of scattering strength with frequency, and are associated with refractive scintillation in the regime of strong scattering. Such scattering occurs when the Fresnel scale $r_{\rm F}$ exceeds the diffractive scale length, $r_{\rm diff}$, the transverse length scale over which the mean square difference in phase delay imposed by plasma inhomogeneities in the ISM is one radian. Refractive variations occur on a timescale $\sim r_{\rm F}^2/r_{\rm diff} \equiv r_{\rm ref}$.

A source scintillating in the regime of strong scattering may also exhibit very fast, narrowband intensity variations due to diffractive scintillation. These are routinely observed in pulsars (e.g. Rickett 1970; Ewing et al. 1970). Diffractive scintillation is only observable for source sizes $\theta_{\rm s} \lesssim r_{\rm diff}/z$. This angular size requirement is so stringent that no extragalactic radio source has previously been observed to exhibit diffractive scintillation (Dennison & Condon 1981; Condon & Backer 1975). However, when present, it is identifiable by the fast, narrowband character of its variations, which are distinct from the slow, broadband variations exhibited by weak and refractive scintillation.

In this paper we present the discovery of narrowband, fast scintillation in the quasar J1819+3845 at $\lambda 21$ cm, characteristic of diffractive scintillation, and derive the properties of the source component undergoing this effect. Technical issues related to the reduction of data from this variable source are discussed in the following section. In Sect. 3 we derive the characteristics of the variability and derive the interstellar medium and source parameters associated with the phenomenon. The implications of the discovery are discussed in Sect. 4 and the conclusions are presented in Sect. 5.

2. Observations and reductions

Since its discovery in 1999 J1819+3845 has been observed very regularly with the Westerbork Synthesis Radio Telescope (WSRT). Most observations were obtained at 4.9 GHz but since 2001 we have increased our monitoring at 1.4 GHz as well. Initially 1.4 GHz observations were done with the continuum backend which provides 8 contiguous bands of 10 MHz centered around 1380 MHz. As of July 2002 we have used the new line backend which provides both increased spectral resolution as well as a doubled overall bandwidth. In this paper we report on these wide-band observations that were taken on eleven dates between 14 Jul. 2002 and 30 Jan. 2005. The last three observations were taken with an ultra wide frequency coverage and will be described separately below.

2.1. Wideband (160 MHz) data: July 2002 till Nov. 2003

All observations were continuous over a 12-hour duration. The basic integration time of the WSRT is 10 s but data were averaged for either 30 s or 60 s. The backend was configured to observe simultaneously in eight 20 MHz wide sub-bands centered at 1450, 1428, 1410, 1392, 1370, 1350, 1330/1332 and 1311/1310 MHz. Small gaps around 1381 and 1320 MHz were introduced to avoid occasional RFI at these frequencies. Each sub-band was further subdivided into 64 Hanning-tapered channels yielding 625 kHz spectral resolution. Further processing was performed only on the 28 odd channels from channel 3 to 57. The lower and upper channels at the edges of each subband were discarded because of higher noise levels. Due to human error no spectral tapering was applied to the 22 Feb. 2003 data. To retain full sensitivity channels 3–58 were processed for that epoch. The total overall bandwidth spanned by each subband is 17.5 MHz. Full polarization information was obtained but will be presented elsewhere. The source J1819+3845 shows only very faint (<1%) polarization which did not interfere with the total intensity analysis.

The observations were generally taken under reasonable to fair weather conditions (i.e. no strong winds or precipitation). Continuous radiometry using a frontend noise source on a 10 s time interval provided accurate system temperatures to convert the correlation coefficients to relative flux density. These relative flux densities are converted to absolute flux densities using the primary WSRT flux calibrator 3C 286 which is tied to the Baars et al. (1977) scale, which assumes a flux density of 14.9 Jy for 3C 286 at a frequency of 1380 MHz. The calibration procedure takes the spectral index of 3C 286 at these frequencies (–0.48) into account.

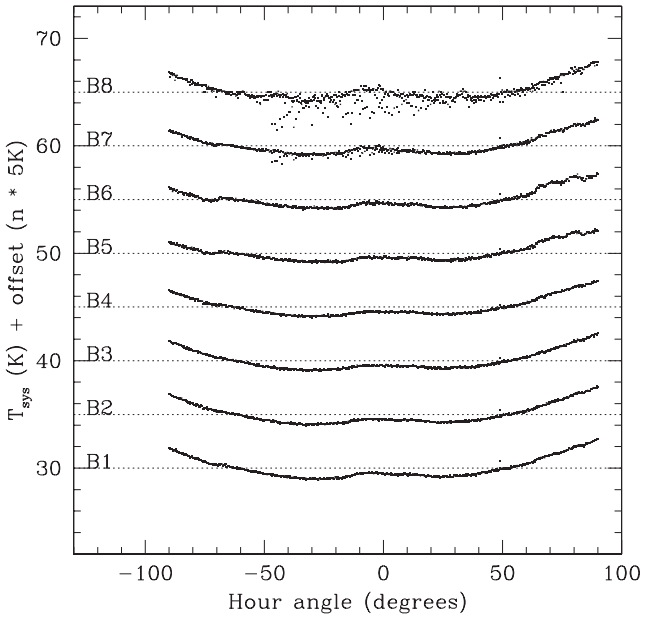

Fig. 1. System temperature for one telescope as a function of hour angle for each of the eight 20 MHz bands. Band 1 is at 1450 MHz, band 8 at 1310 MHz. Each curve was normalized to an average T_{sys} of about 30 K. Different bands are displaced by 5 K. Note the effects of the radar RFI in bands 7 and 8 (see Sect. 2).

A typical example of the run of system temperatures with hour angle is shown in Fig. 1 for one of the 14 telescopes and all 8 frequency bands. A slight non-linearity in the backend leads to a small underestimation of the flux density at the extreme hour angles where the system temperature increases slightly due to increased spillover from ground radiation. We estimate this non-linearity effect to be about 1% at most. (The non-linearity was cured in the late spring of 2004.) Flux density errors due to telescope pointing and telescope gain errors are well below 1% at 1.4 GHz. Overall we therefore believe the flux density scale to be good to 1–2%. This is corroborated by the relative flux density stability of the pairs of calibrator sources observed before and after the 12 h run on J1819+3845 (3C 286/CTD93 before and 3C 48/3C 147 after). We also have long track observations on several known stable sources which agree with our 1% long-term stability assessment.

The determination of weak, rapid intensity fluctuations in a radio source is not trivial when using aperture synthesis techniques at low frequencies, especially in an E-W synthesis array like the WSRT where 12 h is needed to synthesize a good beam. It would seem to violate the principle of "synthesis" which requires a nonvariable sky. However, there are no fundamental limitations in taking care of source variability, as is described by Dennett-Thorpe & de Bruyn (2000, 2003) for data taken on J1819+3845 at a frequency of 4.9 GHz. At 1.4 GHz the situation is more complex. Within the field of view of the array's 25 m dishes several hundred other sources are detected, with flux densities, in addition to the ∼100 mJy of J1819+3845, ranging from 13 mJy to 0.1 mJy. One of the 12 h images is shown in Fig. 3. The noise level in the final images is typically 10–15 μJy per beam.

We have now observed this field about a dozen times at 1.4 GHz. Although the character and magnitude of the variations of J1819+3845 changes significantly, the confusion from the sky is expected, and observed, to be very stable, allowing it to be modelled well. Before vector averaging the visibilities for either 30 s or 60 s time intervals to form the light curve, we removed the response from typically 250 background sources. Any residual confusion from fainter sources is estimated to be less than 1–2 mJy which is typically 1% of the flux density of J1819+3845. More importantly, for the present study, is that these residual effects are broadband in nature and would be very similar from epoch to epoch (because the uv-coverage is very similar). We are therefore certain that the observed fast and spectral variations are not due to background confusion and must be due to the properties of the source and the interstellar medium.

With observations spread across all seasons we have of course frequently observed in daytime. The quiet Sun still contributes a strong signal at 21 cm despite the >40 dB attenuation by the primary beam. However, the visibility function of the quiet Sun drops very fast and is undetectable at projected baselines beyond a few 100 m. In a few cases rapid 1–2 mJy fringing was observed and short (≤144 m) baseline visibilities were excluded from the visibility averaging.

The lowest sub-band is intermittently affected by interference due to 1 MHz of spectral overlap with a nearby radar. The radar, which is activated with a period of 9.6 s, beats with a 4-min period when observed with the WSRT, whose noise sources are monitored every 10 s. Close inspection of the data suggests that the band centred on 1311/1310 MHz is most affected, with weak interference also present on the band centred at 1330 MHz (see e.g. Fig. 4, the 22 Feb. 2003 dynamic spectrum). In the calculation of the characteristics of the scintillation signal, data from the entire two lower sub-bands are excluded whenever interference is evident.

Most of the RFI in the two low frequency bands enters the light curves via the system temperature correction procedure. We have therefore also processed in parallel the data without applying this correction. The dynamic spectra for the 1310/1311 MHz band indeed then look much cleaner. To take care of the slight systematic system temperature variation with hour angle the data for February and April 2003 shown in Fig. 4 were corrected using the uncontaminated Tsys curves for the higher frequency bands.

In order to ascertain the accuracy of the overall amplitude calibration on a range of timescales, we have also reduced a 10 h observation of the bright stable radio source CTD93, observed in May 2003 with a similar instrumental setup as J1819+3845. The power spectrum of the temporal fluctuations of this source is shown in Fig. 2 after scaling the intensity to a mean flux of 100 mJy. This means that the thermal noise has been reduced to an insignificant level and we are left with the combined variations due to atmospheric opacity, pointing and amplitude calibration. The level of "variability" observed in CTD93 on frequencies of <0.001 rad/s, which correspond to timescales of about 10 m to 2 h, is significantly less than 1%. On faster timescales this drops to about 0.1%, a level probably set by the total power amplitude calibration. All fluctuations

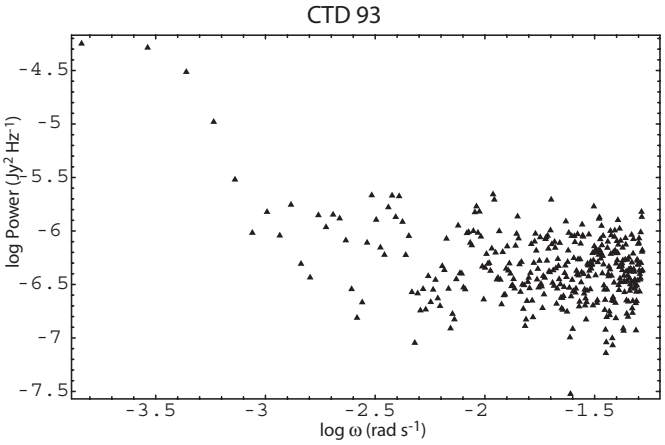

Fig. 2. The power spectrum of temporal variations from a 10-h observation of the stable bright radio source CTD 93. In order to compare with the temporal variations in J1819+3845, the power spectrum is computed from a light curve in which the flux densities have been reduced (by a factor ∼50) to have a mean of 100 mJy (see Sect. 2).

observed in J1819+3845 appear to be significantly in excess of these levels, at any temporal scale, and become thermal noise limited at the fastest timescales sampled.

2.2. Ultra wideband (∼600 MHz) data: Jan. 2004 to Jan. 2005

As of Jan 2004 the WSRT online software allowed frequency switching with high efficiency between different frequency settings within the L-band receiver which covers the range from 1150–1800 MHz. Although a significant fraction of this band is affected by man-made interference – GPS, GLONASS and geostationary satellites – the advantage of the wider band to study the spectral decorrelation effects of the scintillations more than outweighed this loss of data. Three observations were taken with this ultra wideband setup, which had the following switching scheme: at intervals of 60 s we switched between different frequency "combs" of 8 adjacent 20 MHz bands. For every comb the first 20 s of data had to be discarded leaving 40 s of good data. The observations of 25 Jan. 2004 and 12 April 2004 were carried out with three frequency combs but different central frequencies. In the most recent data of 30 Jan. 2005 we used 4 combs almost completely covering the available *L*-band frequency range. After calibration and RFI editing the data were averaged over 40 s timeslots leading to light curves sampled on a regular 180 s or 240 s grid.

The strong RFI encountered in several bands of each comb made it impossible to provide a reliable intensity calibration. The decomposition of the total power radiometric data into system temperatures and electronic gains requires stable conditions during a 10 s period, which is obviously not the case under strong and impulsive RFI conditions. The effects of this on the amplitude stability were exacerbated by the small linearity problem in the receiver. The ultra-wideband data were therefore internally calibrated on a band-by-band basis for each band of the frequency combs by normalizing on the 12-h averaged flux of J1819+3845 itself.

3. Results and analysis

The dynamic spectra displayed in Figs. 4 and 5 present a concise summary of the intensity fluctuations exhibited by J1819+3845 over all eleven epochs of our observations. The variations exhibit fine structure in both time and frequency. The spectral features are stochastic in nature, as both fading and brightening streaks are visible in all dynamic spectra. The spectral structure is associated with the fastest variations visible during each epoch. This is particularly apparent during the 22 Feb. 2003 and 12 Apr. 2003 observations, in which variations occur on timescales as short as 20 min, but are as long as several hours at other times of the year, with a variation being defined here as a complete oscillation in the light curve. The reduced duty cycle (40 s of data for every 180 s or 240 s) in the frequency-mosaiced dynamic spectra in Fig. 5 means that some of the fine temporal structure evident in other observations (cf. 22 Feb. 2003, 12 Apr. 2003) would not be as easily detectable in these observations. A very recent regular 160 MHz observation (taken on 28 Mar. 2005), not presented here shows that such fine structure is still present. A more detailed analysis of variations in the 21 cm band over a period of 6 years will be presented in de Bruyn et al. (in preparation).

The light curves shown in Fig. 6 further indicate that the intensity variations occur on several timescales and that these timescales change as a function of observing epoch. This is also demonstrated by the power spectra of the intensity fluctuations shown in Fig. 7. The light curves from which these power spectra were computed contained no gaps over the 12 h duration of the observation, with flux densities sampled every 60 s.

We discuss the temporal variability in Sect. 3.1 and the spectral characteristics in Sect. 3.2. These are used to derive parameters of the source and scattering medium in Sect. 3.3.

3.1. Timescales

Here we compare the observed power spectrum of temporal intensity variations to models for refractive scintillation. We argue that refractive scintillation fails to account for much of the variation observed on timescales shorter than 6 h.

The scintillation velocity is fastest in the period December-April (Dennett-Thorpe & de Bruyn 2003), so the 22 Feb. 2003 and 12 Apr. 2003 datasets, which exhibit the fastest intensity variations, are the most useful in understanding the temporal characteristics of the variations. Figures 4 and 6 clearly demonstrate that, for both datasets, narrowband (∼160 MHz), ∼20−120-min variations are superposed on slower ∼6-hourly variations. (The frequency-mosaiced observations made on similar dates in 2004 and 2005 are less suitable because their time-sampling is irregular, and their decreased S/N (per frequency channel) renders them unsuitable for characterising any fast, low-amplitude intensity fluctuations.)

The variations on timescales $\gtrsim$6 h match those expected from refractive scintillation on the basis of observations at higher frequencies. The transition between and strong scattering is thought to occur in the range $\gtrsim$3.5−5 GHz for this source (Dennett-Thorpe & de Bruyn 2000) and the intensity variations observed at 4.9 GHz are attributed to a scattering

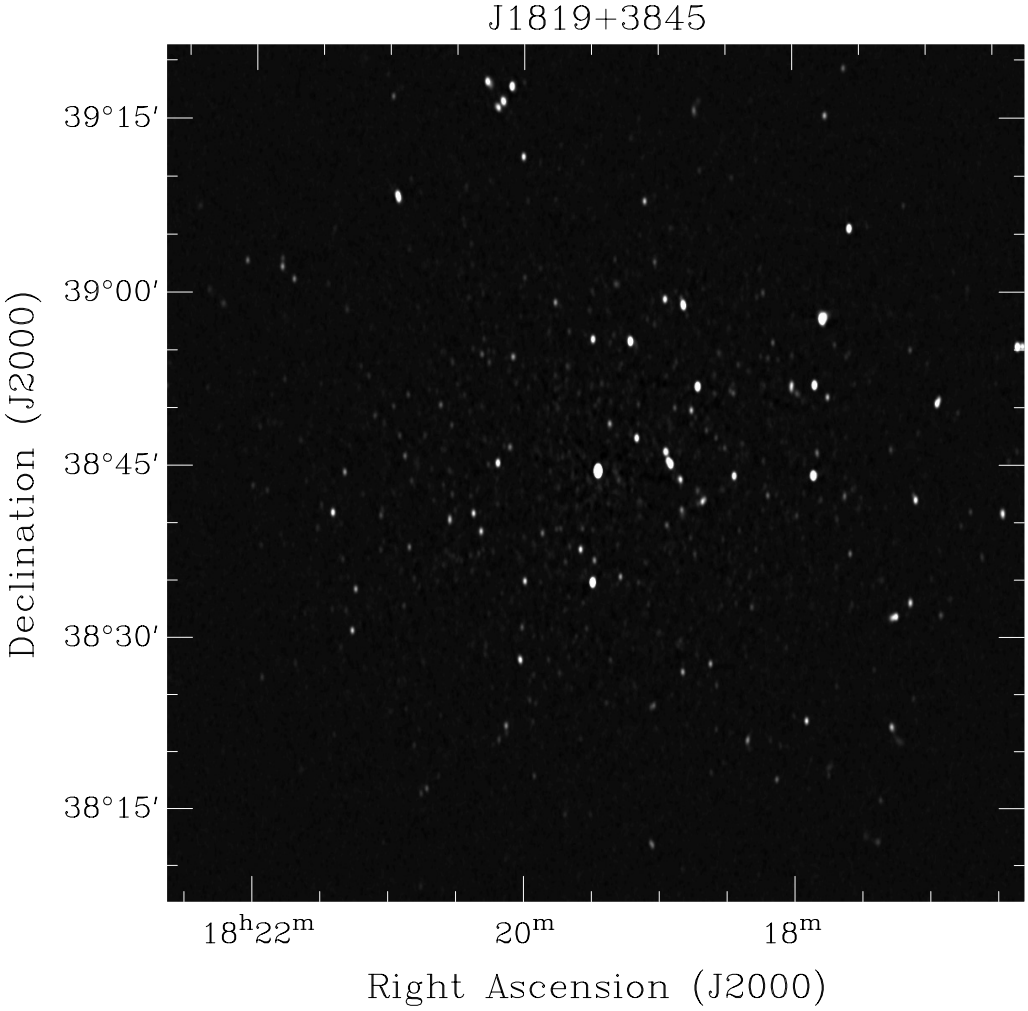

Fig. 3. The field surrounding J1819+3845 as observed on 22 August 2003 at 21 cm.

screen ∼15 pc from Earth, with $v_{\rm ISS} \approx 50\,{\rm km\,s^{-1}}$. On this basis and assuming Kolmogorov turbulence one predicts the refractive scintillation timescale at 1.4 GHz to be between 4 and 8 h, consistent with the slow variations observed here.

The larger duration of the frequency-dependent scintles observed during other epochs, their lack of associated large broadband flux density deviations and the increased timescale of the fine, frequency-dependent structure suggests that the refractive scintillation timescale exceeds the 12-h span of these observations. This is expected on the basis of the slow-down observed in the variations at 6 cm during this period.

Figure 6 displays the variations seen at 1.4 GHz with those observed at 4.9 GHz during the same period. This demonstrates an excess of variability on short (20–120 min) timescales at 1.4 GHz. It is difficult to account for this excess in terms of refractive scintillation alone, since the timescale of the variations increases sharply ($\propto\lambda^{2.2}$ (e.g. Narayan 1992; Armstrong et al. 1995)) in the regime of strong scattering.

To further illustrate the difficulty of accounting for all of the power observed in the short timescale variations in terms of refractive scintillation, we consider two quantitative models for the power spectrum of refractive variability: scintillation (i) from a thin phase-changing screen and (ii) from an extended medium in which the source size exceeds the refractive scale (i.e. $\theta_{\rm src} > \theta_{\rm ref}$).

The temporal power spectrum due to refractive scintillation caused by a thin screen of scattering material is (Codona & Frehlich 1987)

$$\Phi_I(\omega) = \frac{4\,r_{\rm e}^2\,\lambda^2 I_{\rm src}^2\,\Delta L}{v_{\rm ISS}} \int {\rm d}\kappa_y \Phi_{\rm N_e}\left(\frac{\omega}{v_{\rm ISS}}, \kappa_y\right) \left| V\left(\frac{\omega\, z}{v_{\rm ISS}\, k}, \frac{\kappa_y z}{k}\right)\right|^2 \times \sin^2\left[\frac{\left(\frac{\omega^2}{v_{\rm ISS}^2} + \kappa_y^2\right) z}{2k}\right] \exp\left[-D_\phi\left(\frac{\omega\, z}{v_{\rm ISS}\, k}, \frac{\kappa_y z}{k}\right)\right], \quad (1)$$

where ω is the angular frequency, κ_x and κ_y are spatial wavenumbers, $\Phi_{\rm N_e}(\kappa_x, \kappa_y)$ is the power spectrum of electron density fluctuations, z is the distance to the scattering medium, $\Delta L \ll z$ is the screen thickness, $r_{\rm e}$ is the classical electron radius, $V(\boldsymbol{r})$ is the visibility of the source and $D_\phi(\boldsymbol{r})$ is the phase structure function. Only the source visibility can counteract the sharp decline in the power spectrum due to the exponential function at $\omega > v_{\rm ISS}/r_{\rm ref}$, but this requires a visibility that *rises* nearly exponentially quickly to account for the observed shallow of the decline of power spectrum (see Fig. 7).

The refractive power spectrum for a scattering medium distributed along the line of sight declines more slowly at high

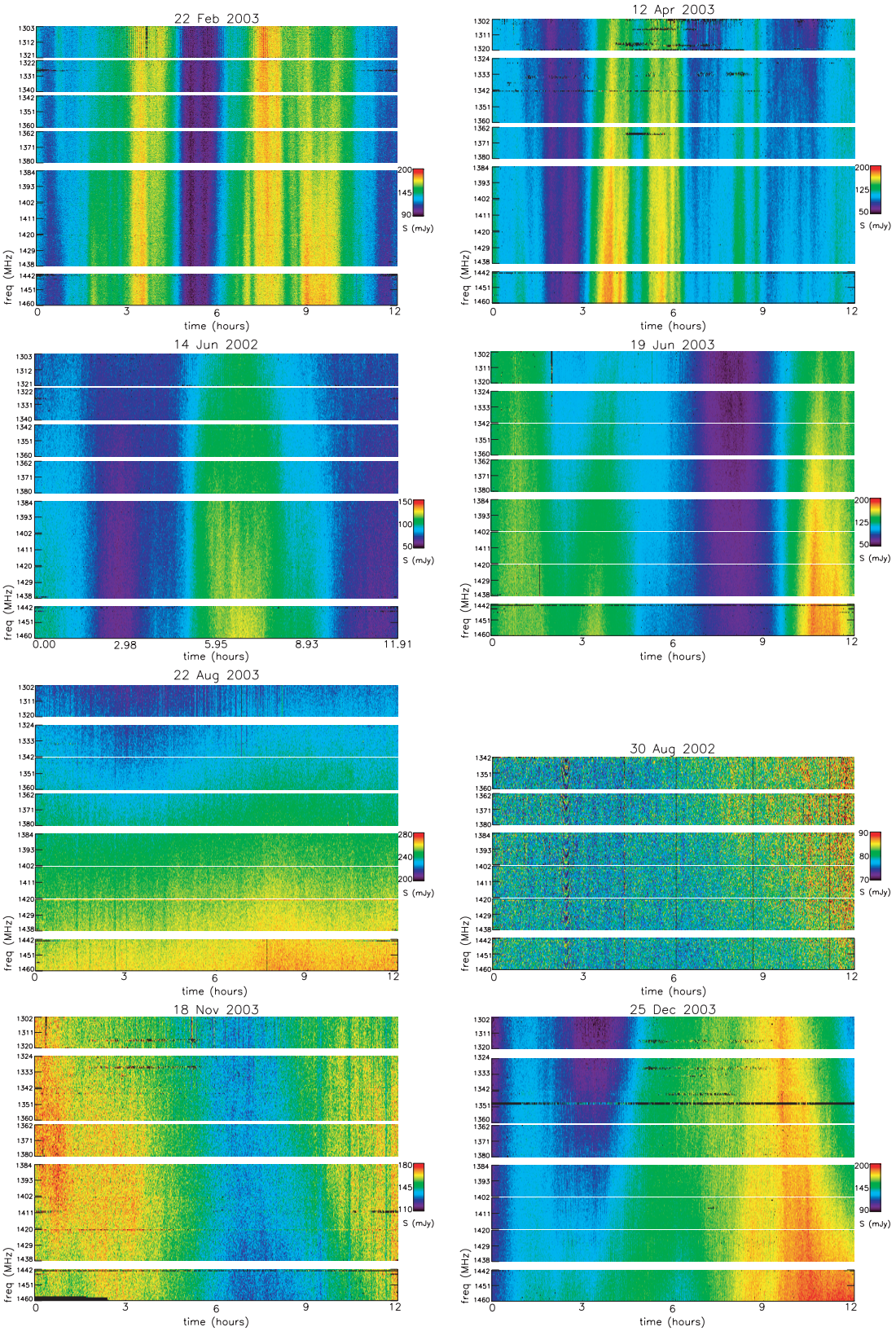

Fig. 4. The dynamic spectrum of J1819+3845 over 160 MHz on eight epochs in the interval Jun. 2002–Dec. 2003, arranged by day of year, given above the panels. Each point in each dynamic spectrum represents a one minute average over a 625 kHz bandwidth. Bad data flagged in the analysis are represented by black points. The periodic fringes visible in the lowest frequency band on 22 Feb. 2003 and 12 Apr. 2003 are caused by terrestrial interference. Note that the displayed flux density range in some epochs when the source is not strongly variable (e.g. 30 Aug. 2002) is rather small, making the dynamic spectrum appear more noisy. (This figure is available in colour in electronic form.)

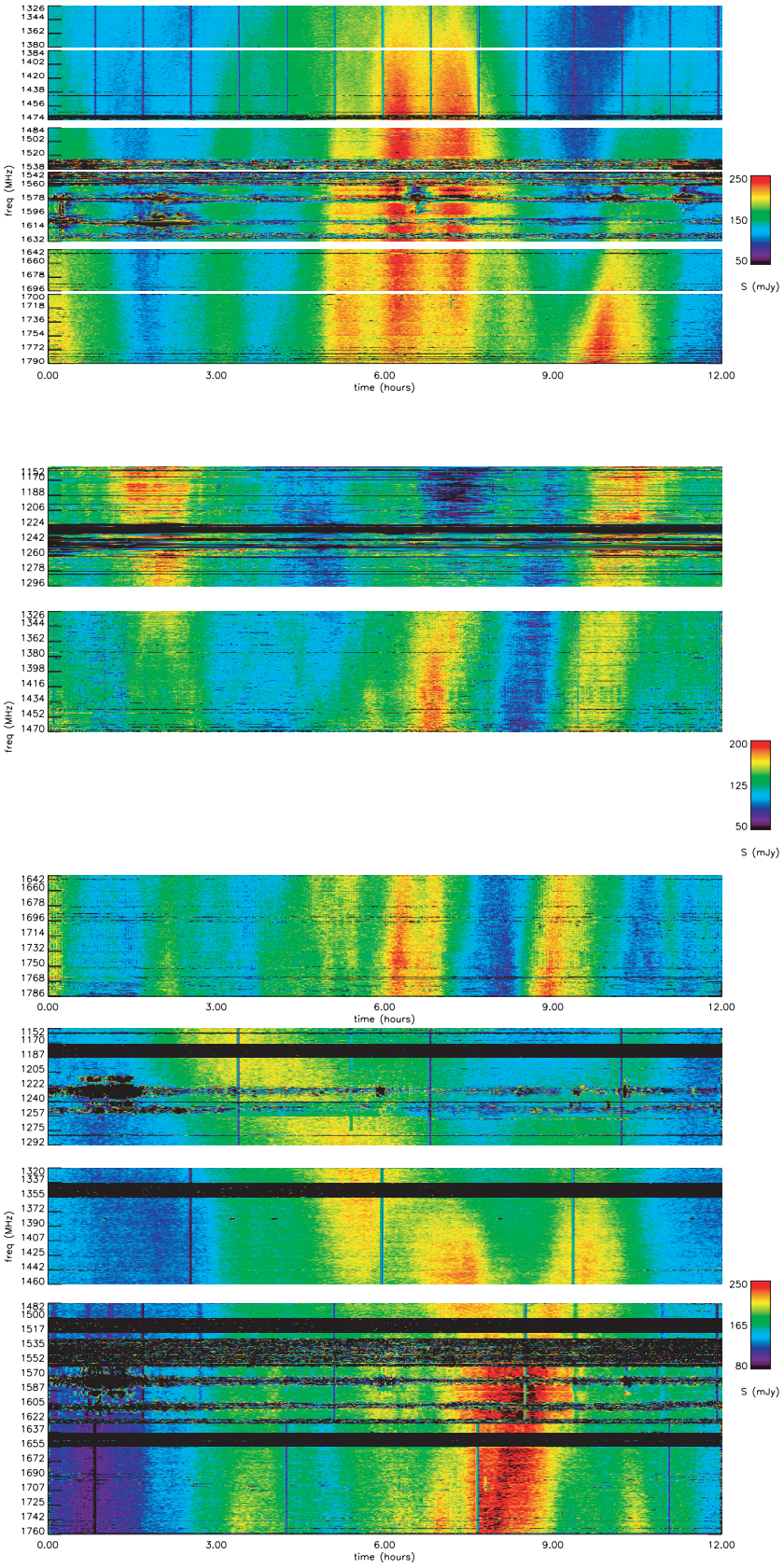

Fig. 5. Wideband, frequency-mosaiced observations of the scintillation spectrum in J1819+3845 on 25 Jan. 2004 (top), 12 Apr. 2004 (middle) and 30 Jan. 2005. The sizes of the white vertical spaces between data channels are proportional to their corresponding frequency gaps. Bad data points, channels or bands are marked by black pixels. The contribution of the intrinsic spectrum of J 1819+3845 has been removed by normalising each spectral channel so that they are identical (and equal to the mean source flux density, averaged over the entire dynamic spectrum). (This figure is available in colour in electronic form.)

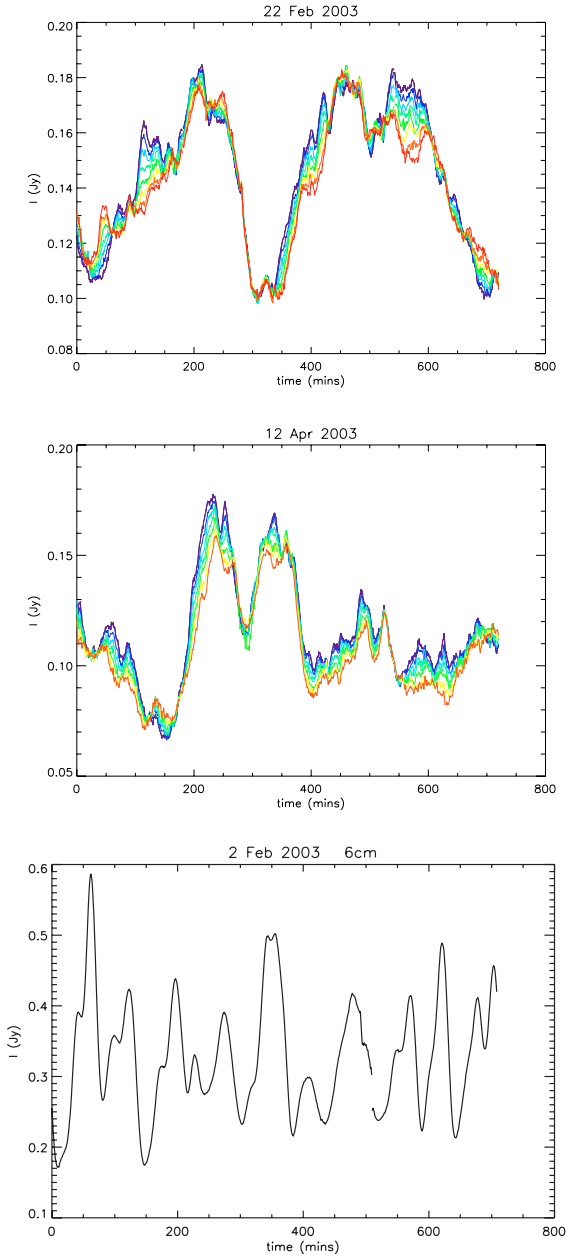

Fig. 6. Light curves of the variability on 22 Feb. 2003 and 12 Apr. 2003 at 1.4 GHz in each band. The (colour-coded) light curves from individual bands differ on timescales ranging from 20 mins up to several hours. The variations at the lowest frequency band in the 12 Apr. 2003 dataset were contaminated by terrestrial interference, and are excluded from this plot. The observing frequency increases with colour from red to blue. The differences between the band light curves are well above the 1 mJy noise level (per 60 s). The bottom panel, a light curve of the source at 4.8 GHz on 2 Feb. 2003, contrasts the smoothness of the intensity variations observed in the regime of weak scattering with those observed at 21 cm. The noise on the 4.8 GHz light curve is typically 1% of the flux density or less. These errors are discussed in Dennett-Thorpe & de Bruyn (2003) in detail. (This figure is available in colour in electronic form.)

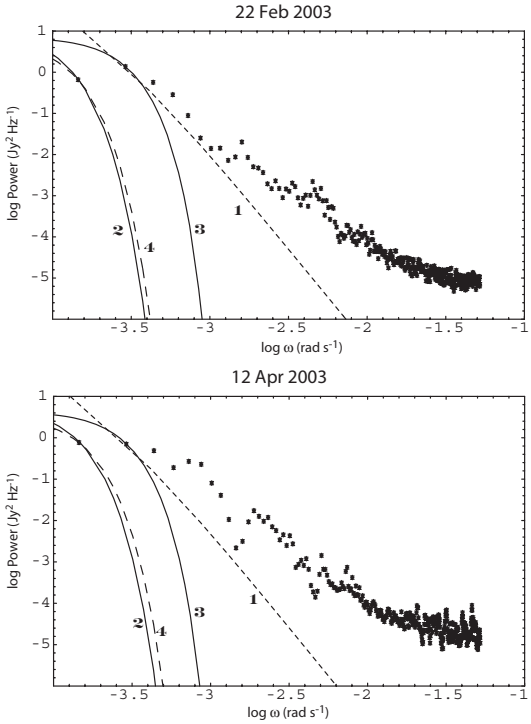

Fig. 7. The average power spectra of the temporal variations on 22 Feb. 2003 (*top*) and 12 Apr. 2003 (*bottom*) shown with the expected thin screen and extended medium power spectra for comparison. The lines are labelled according to the model: (1) best-fitting extended medium with medium scale length 15 pc, (2) thin screen model with $z = 15$ pc with $C_N^2 \Delta L$ adjusted to match the power at the lowest frequency bin (3) same as (2) but with $C_N^2 \Delta L$ adjusted to match the power at the second-lowest frequency bin and (4) a thin screen model with $z = 4$ pc with $C_N^2 \Delta L$ chosen to match the power at the lowest frequency bin. A scintillation speed $v_{\rm ISS} = 50\,{\rm km\,s^{-1}}$ is assumed. Spectra matched to the second lowest point are shown because they exhibit more power at high frequencies. However, even for this conservative choice they do not replicate the observed power at high frequencies. In all models all of the source flux density is assumed to undergo scintillation. For the thin-screen model a point source is assumed; a source of finite size further decreases the power at high frequency. In the extended medium model used here, the form of the power spectrum is valid for $\theta_{\rm src} > \theta_{\rm scat}$, so we choose $\theta_{\rm src} = 1.0$ mas. However, the curves shown here differ little from ones in which the model is stretched by using $\theta_{\rm src} = 0.1$ mas instead. The parameters of the fits are summarised in Table 1. A minimum bias filter (Papoulis 1991, pp. 445–455) has been applied to the spectra in order to reduce the errors inherent in the spectral estimation, however the error bars shown are not mutually independent.

temporal frequencies. For a source of angular size $\theta_{\rm src} \gtrsim \theta_{\rm ref}$ scattered in a medium with thickness L and distributed according to $C_N^2(z) = C_N^2(0)\exp(-z^2/L^2)$ (with z measured from the observer) the power spectrum of intensity fluctuations is (Coles et al. 1987)

$$\phi_I(\omega) = \frac{2\sqrt{\pi}\, r_{\rm e}^2 \lambda^2 L\, I_{\rm src}^2}{v_{\rm ISS}} \int {\rm d}\kappa_y \Phi_{\rm N_e}\left(\frac{\omega}{v_{\rm ISS}}, \kappa_y\right) \times \frac{1 - \exp\left[-\frac{(\omega^2/v_{\rm ISS}^2+\kappa_y^2)^2 r_{\rm F}^4}{4[1+(\omega^2/v_{\rm ISS}^2+\kappa_y^2)L^2\theta_{\rm s}^2/2]}\right]}{\sqrt{1+\left(\frac{\omega^2}{v_{\rm ISS}^2}+\kappa_y^2\right)L^2\theta_{\rm s}^2/2}}. \quad (2)$$

For a Kolmogorov spectrum of turbulent fluctuations this power spectrum declines asymptotically as $\sim(v_{\rm ISS}/\omega)^{8/3}$.

Table 1. Parameters used in the fits to the temporal power spectra in Fig. 7. The transition frequency between weak and strong scattering for $C_N^2 L = 1.42 \times 10^{17}$ at $z = 4$ pc is 5.45 GHz and for $z = 15$ pc $C_N^2 L$ values of 1.82×10^{16} and 3.69×10^{15} m$^{-17/3}$ correspond to transition frequencies of 3.89 and 2.22 GHz respectively.

	22 Feb. 2003	12 Apr. 2003
$z = 15$ pc thin screen matching lowest frequency power	$C_N^2 L = 1.82 \times 10^{16}$ m$^{-17/3}$	$C_N^2 L = 1.38 \times 10^{16}$ m$^{-17/3}$
$z = 4$ pc thin screen matching lowest frequency power	$C_N^2 L = 1.42 \times 10^{17}$ m$^{-17/3}$	$C_N^2 L = 1.01 \times 10^{17}$ m$^{-17/3}$
$z = 15$ pc thin screen matching second lowest frequency power	$C_N^2 L = 3.69 \times 10^{15}$ m$^{-17/3}$	$C_N^2 L = 4.0 \times 10^{15}$ m$^{-17/3}$
extended medium ($\Delta L = 15$ pc)	$C_N^2 = 10^{-3.18}$ m$^{-20/3}$	$C_N^2 = 10^{-3.25}$ m$^{-20/3}$

Figure 7 illustrates the excess of power observed on short timescales relative to that expected from the two refractive scintillation models discussed here. The fitted models assume a scintillation speed $v_{\rm ISS} = 50\,{\rm km\,s^{-1}}$ and that all of the source emission is compact enough to be subject to interstellar scintillation (i.e. there are no $\gtrsim$5 mas features in the source). The fit parameters are listed in Table 1. The level of fluctuations on timescales of less than $\sim$2 h, which the dynamic spectra show to be associated with highly frequency dependent variations, are difficult to explain in terms of refractive scintillation, suggesting that their origin is most likely diffractive in nature.

3.2. Spectral decorrelation of the scintillation signal

The spectral characteristics of the scintillation signal are determined by computing the autocovariance of the intensity variations across the observing band, $C_\nu(\Delta\nu) = \langle I(\nu+\Delta\nu)I(\nu)\rangle - \bar{I}^2$.

In order to isolate the spectral decorrelation due to the narrowband fluctuations only, it is necessary to remove the appreciable variation in the mean (intrinsic) source flux density across our observing bandwidth. This is removed by "flat-fielding" the spectrum prior to autocorrelation. The dynamic spectrum is normalised so that the time-average flux density in each spectral channel is identical, and equal to the flux density averaged across the entire dynamic spectrum. This prevents the mean spectral slope across the band from masquerading as a scintillation signal and weights intensity fluctuations across the entire spectrum fairly, provided that the spectrum of the narrowband variations resembles the overall source spectrum. Although this spectral match may only be approximate in practice, the normalisation is sufficient for present purposes since the contribution to the error caused by any small spectral index mismatch is also small[1]. The effects of spectral misestimation are incorporated in the error budget when considering fits to the autocorrelation functions in Sect. 3.3 below.

The short timescale of the scintillation requires that C_ν be computed for each one-minute time slot individually. The final frequency autocorrelation function is the average of the 710−720 functions computed separately from each time slot.

[1] The error is no larger than the mean square of the flux density error; the contribution cancels to first order in flux density difference since the autocorrelation averages out the contributions from both higher and lower frequencies. For instance, the additional contribution to the autocorrelation is $\sim$0.1 mJy^2 across 100 MHz for a diffractively scintillating component of spectral index 1.0 and a source with spectral index 0.3.

The autocovariances for the 25 Jan. 2004, 12 Apr. 2004 and 30 Jan. 2005 observations are shown in Fig. 9. These datasets are used because they span a sufficiently large spectral range that they encompass the bandwidth of the scintillation structure. The error in our sample autocorrelation function, depicted by the grey region in Fig. 9, incorporates the fact that our observations sample a finite number of scintles both in time and frequency (see Appendix A).

Can refractive scintillation alone account for the spectral structure? No calculation of the form of the spectral decorrelation due to refractive scintillation exists in the literature, but refractive scintillation is known to decorrelate on a bandwidth comparable to the observing frequency: $\Delta\nu_{\rm ref} \sim \nu$ (e.g. Goodman & Narayan 1989). We can make a simple estimate of the importance of refractive intensity variations by following the simple geometric optics model described in Narayan (1992). The amplitude of a typical flux variation depends on the root-mean-square focal length of phase fluctuations on scales $r_{\rm ref}$ in the scattering medium. Since the focal length is much larger than the distance to the observer, and assuming Kolmogorov turbulence, the amplitude is $\sim r_{\rm diff}^{1/3}(z/k)^{-1/6}$. Thus the expected flux density change across a bandwidth $\Delta\nu$ is $\Delta S(1+\Delta\nu/\nu)^{17/30} - \Delta S$, where $\Delta S \approx 25$ mJy is the root-mean square amplitude of the refractive scintillations. Thus the contribution due to refractive frequency variations is at most 2.0 mJy across a bandwidth of 200 MHz, considerably smaller than the variation observed.

Larger chromatic effects are possible if a strongly refracting "wedge" or prism of interstellar material is present along the line of sight. Chromatic refraction due to a wedge would be important if its gradient were sufficient to change the angle of refraction from the low to high edge of the observing band by an amount comparable to $\theta_{\rm ref}$. However, if the gradient is not perfectly aligned orthogonal to the direction of the scintillation velocity one expects the scintillations to be displaced in time as well as frequency. The wedge would have to displace the scintillation pattern by a relative distance $\gtrsim 0.3\, r_{\rm ref}$ from one edge of the observing band to the other to account for the chromatic nature of the intensity fluctuations observed here. One would then expect the wedge to also displace the scintillations in time by $\gtrsim 0.3\, t_{\rm ref}$ as one moves across the observing band. No such temporal displacement is observed. Moreover, as the scintillation velocity changes through the year, one would expect a systematic change in the slope of the frequency-dependent scintles (i.e. $\mathrm{d}\nu/\mathrm{d}t$) with a change in the direction of the scintillation velocity. As no systematic change with scintillation velocity is

observed, we conclude that there is no spectral contamination due to a refracting wedge.

3.3. Diffractive scintillation source characteristics

The temporal and spectral characteristics of the intensity variations are combined to determine the parameters of the source undergoing diffractive scintillation. We concentrate on fits to the spectral decorrelation of the 25 Jan. 2004, 12 Apr. 2004 and 30 Jan. 2005 datasets where the spectral coverage exceeds the typical bandwidth of the scintillation structure.

A detailed interpretation of the scintillation parameters depends in detail on whether the scattering material is located in a thin layer or whether it is extended along the ray path. The manner in which the scale size of the scintillation pattern and the form of the spectral decorrelation are altered by source size effects depends on the distribution of scattering material along the line of sight. We consider two specific models, one in which the scattering material is confined to a thin screen a distance z from the observer, and the other in which the scattering material is extended homogeneously out to a distance Δz from the observer.

In the thin screen model the spectral autocorrelation takes the form (Chashei & Shishov 1976; Gwinn et al. 1998)

$$F_{\rm thin} = A_{\rm off} + S^2_{\rm diff}\left(1 + \frac{\theta_0^2}{\theta_{\rm cr}^2} + \frac{\Delta\nu^2}{\Delta\nu_{\rm t}^2}\right)^{-1}, \quad (3)$$

where $S_{\rm diff}$ is the flux density of the source component exhibiting diffractive scintillation, $\Delta\nu_{\rm t} = \nu r_{\rm diff}^2/r_{\rm F}^2$ is the decorrelation bandwidth that a *point source* would possess in this scattering medium, and $\theta_0/\theta_{\rm cr}$ is the ratio of the source angular radius to a critical angular scale of the scintillation pattern $\theta_{\rm cr} = r_{\rm diff}/2z$. Equation (3) was first derived for Gaussian turbulence but it has also been derived approximately for Kolmogorov turbulence (Gwinn et al. 1998). The spectral autocorrelation in the thin screen model is degenerate to the combination S, $\Delta\nu_{\rm t}$ and $\theta_0/\theta_{\rm cr}$, so it is only possible to fit for two of these three parameters. The uncertainty in the base level of the observed spectral autocorrelation function necessitates the introduction of the additional constant $A_{\rm off}$. When the source size exceeds the critical angular scale $\theta_{\rm cr}$ the form of the spectral decorrelation simplifies to

$$F_{\rm thin} \approx A_{\rm off} + S^2_{\rm diff}\begin{cases}\left(\frac{\theta_0}{\theta_{\rm cr}}\right)^2, & \Delta\nu \lesssim \Delta\nu_{\rm t}\frac{\theta_0}{\theta_{\rm cr}} \\ \left(1+\frac{\Delta\nu^2}{\Delta\nu_{\rm t}^2}\right)^{-1}, & \Delta\nu \gtrsim \Delta\nu_{\rm t}\frac{\theta_0}{\theta_{\rm cr}}\end{cases}. \quad (4)$$

The characteristic scale of the frequency pattern is thus set by the source size to

$$\Delta\nu = \Delta\nu_{\rm t}\left(\frac{\theta_0}{\theta_{\rm cr}}\right). \quad (5)$$

The scale of the observed diffractive scintillation pattern is

$$s_0 = r_{\rm diff}\sqrt{1+\left(\frac{\theta_0}{\theta_{\rm cr}}\right)^2}. \quad (6)$$

This scale can be equated directly to the product of the diffractive scintillation timescale and velocity, $v_{\rm ISS}\, t_{\rm diff}$. A notable feature of the thin-screen model is that the pattern scale grows arbitrarily large with source size.

The spectral decorrelation associated with the extended medium model is (Chashei & Shishov 1976),

$$F_{\rm ex} = A_{\rm off} + S^2_{\rm diff}\, R(\Delta\nu)\left[1 + f(\Delta\nu)\frac{\theta_0^2}{\theta_{\rm cr}^2}\right]^{-1}, \quad (7)$$

$$\text{where } f(\Delta\nu) = 2\left(\frac{\Delta\nu_{\rm ex}}{\Delta\nu}\right)^{\frac{3}{2}}\frac{\sinh\left(\sqrt{\frac{\Delta\nu}{\Delta\nu_{\rm ex}}}\right) - \sin\left(\sqrt{\frac{\Delta\nu}{\Delta\nu_{\rm ex}}}\right)}{\cosh\left(\sqrt{\frac{\Delta\nu}{\Delta\nu_{\rm ex}}}\right) + \cos\left(\sqrt{\frac{\Delta\nu}{\Delta\nu_{\rm ex}}}\right)},$$

$$R(\Delta\nu) = 2\left[\cosh\left(\sqrt{\frac{\Delta\nu}{\Delta\nu_{\rm ex}}}\right) + \cos\left(\sqrt{\frac{\Delta\nu}{\Delta\nu_{\rm ex}}}\right)\right]^{-1}, \quad (8)$$

where the point-source decorrelation bandwidth is $\Delta\nu_{\rm ext} = \pi\nu k r_{\rm diff}^2/\Delta z$. When the source is extended the spectral decorrelation function is nearly degenerate to a combination of the free parameters, but it takes the following simple form

$$F_{\rm ex} \approx A_{\rm off} + S^2_{\rm diff}\begin{cases}3\left(\frac{\theta_{\rm cr}}{\theta_0^2}\right)^2, & \Delta\nu \ll \Delta\nu_{\rm ex} \\ \frac{R(\Delta\nu)}{2}\left(\frac{\Delta\nu_{\rm ex}}{\Delta\nu}\right)^{\frac{3}{2}}\left(\frac{\theta_{\rm cr}}{\theta_0}\right)^2, & \Delta\nu_{\rm ex} \lesssim \Delta\nu \lesssim \Delta\nu_{\rm ex}\left(\frac{\theta_0}{\theta_{\rm cr}}\right)^{\frac{4}{3}} \\ R(\Delta\nu), & \Delta\nu \gg \Delta\nu_{\rm ex}\left(\frac{\theta_0}{\theta_{\rm cr}}\right)^{\frac{4}{3}}.\end{cases} \quad (9)$$

Source size reduces the overall amplitude of the spectral autocorrelation function by a factor $\theta_0^2/\theta_{\rm cr}^2$. The diffractive pattern scale is largely insensitive to source size, and grows to a maximum of only twice the diffractive scale length as the source size increases:

$$s_0 = r_{\rm diff}\sqrt{\frac{1+\frac{1}{3}\left(\frac{\theta_0}{\theta_{\rm cr}}\right)^2}{1+\frac{1}{12}\left(\frac{\theta_0}{\theta_{\rm cr}}\right)^2}}. \quad (10)$$

Both models assume that $\theta_0/\theta_{\rm cr}$ is a constant and do not account for any possible variation of source size relative to the critical angle, $\theta_{\rm cr}$, with frequency. Both also assume a circularly symmetric source and an isotropic scattering medium, the implications of which are discussed further below.

3.3.1. Simple brightness temperature estimate

The size of the feature associated with the narrowband intensity fluctuations can be estimated in a simple manner for the thin screen model given the transition frequency and the distance to the scattering screen. The transition frequency, $\nu_{\rm t}$, can be deduced from fits to the refractive power spectrum given the distance to the scattering medium and the scintillation speed (Fig. 7 and Table 1). Dennett-Thorpe & de Bruyn (2003) argue that the screen distance is in the range $z = 4{-}12$ pc. We estimate the brightness temperature for screen distances of 4 and 15 pc assuming a scintillation speed of $v_{\rm ISS} = 50\,{\rm km\,s^{-1}}$, a value deduced on the basis of measurements at 6 cm (Dennett-Thorpe & de Bruyn 2003).

The amplitude of the frequency-dependent scintillation is 20 mJy and its decorrelation bandwidth is 170 MHz

Table 2. Fit parameters with formal 1σ errors from the fit. † Strong RFI affected the spectral normalization of the 12 Apr. 2004 observation, which in turn affected estimation of the frequency autocovariance upon which this fit is based.

	Fit parameter	25 Jan. 2004	12 Apr. 2004†	30 Jan. 2005
Thin screen	Offset $A_{\rm off}$ (Jy^2)	$-3.46 \pm 0.03 \times 10^{-4}$	$-2.98 \pm 0.04 \times 10^{-4}$	$-2.93 \pm 0.02 \times 10^{-4}$
	Bandwidth $\Delta\nu_{\rm t} S_{\rm diff}$ (MHz Jy)	4.09 ± 0.05	4.68 ± 0.07	3.89 ± 0.03
	Size $(1+\theta_0^2/\theta_{\rm cr}^2) S_{\rm diff}^{-2}$ (Jy^{-2})	1740 ± 10	1680 ± 20	1600 ± 10
Extended medium	Offset $A_{\rm off}$ (Jy^2)	$-3.10 \pm 0.03 \times 10^{-4}$	$-2.60 \pm 0.04 \times 10^{-4}$	$-3.06 \pm 0.02 \times 10^{-4}$
	Component flux density and source size $S_{\rm diff}^2 \theta_{\rm cr}^2/\theta_0^2$ (Jy^2)	$1.78 \pm 0.01 \times 10^{-4}$	$1.81 \pm 0.02 \times 10^{-4}$	$2.11 \pm 0.01 \times 10^{-4}$
	Bandwidth $\Delta\nu_{\rm ext}$ (MHz)	5.91 ± 0.07	6.7 ± 0.1	5.91 ± 0.06

(see Fig. 9). The flux density associated with the scintillating component is $S_\nu \approx 20/(\theta_0/\theta_{\rm cr})$ mJy. The ratio $(\theta_0/\theta_{\rm cr})$ is estimated directly from the ratio of the observed to point source decorrelation bandwidth by employing Eq. (5). This equation is valid in the present case since the observed decorrelation bandwidth is several times larger than the point source decorrelation bandwidth for the expected value of $\nu_{\rm t} \gtrsim 4$ GHz (see Table 1). The critical angular scale $\theta_{\rm cr}$ is estimated directly from the scattering screen distance and the transition frequency. One solves for θ_0 using $\theta_{\rm cr}$ and the ratio $\theta_0/\theta_{\rm cr}$ to obtain,

$$\theta_{\rm src} = 7.4 \left(\frac{z}{1\,{\rm pc}}\right)^{-1/2} \left(\frac{\nu_{\rm t}}{1\,{\rm GHz}}\right)^{17/10} \mu{\rm as}. \quad (11)$$

We use the fits to the refractive power spectrum in Fig. 7 to estimate the transition frequency. For $z = 15$ pc one has $\nu_{\rm t} = 3.89$ GHz and $r_{\rm diff} = 2.19 \times 10^7$ m at 1.4 GHz and the expected decorrelation bandwidth of a point source at 1.4 GHz is 43.3 MHz. The corresponding numbers for a screen at $z = 4$ pc are $\nu_{\rm t} = 5.45$ GHz, $r_{\rm diff} = 6.39 \times 10^6$ m and $\nu_{\rm dc} = 13.8$ MHz. For $z = 15$ pc the source size is $\theta_0 = 19\,\mu$as, while for $z = 4$ pc the source size is $67\,\mu$as.

The transition frequency cancels out of the expression for the source brightness temperature leaving,

$$T_{\rm B} = \frac{\lambda^2 S_\nu}{2k_{\rm B}\pi\theta_0^2}(1+z_{\rm S}) = 4.9 \times 10^{12} \left(\frac{z}{1\,{\rm pc}}\right) {\rm K}, \quad (12)$$

where we correct the brightness temperature for the source redshift $z_{\rm S} = 0.54$ and we take $\lambda = 0.21$ m. For $z = 15$ pc the implied brightness temperature is 7×10^{13} K while for $z = 4$ pc it is 2×10^{13} K.

Two factors account for the higher brightness temperature estimated at 1.4 GHz relative to that at 4.9 GHz: (i) the wavelength is 3.5 times larger and (ii) for screen distances $z \approx 15$ pc, the source size is estimated to be up to ∼3 times smaller than the value estimated at 6 cm.

3.3.2. Fits to the spectral autocovariance

For completeness we also estimate the brightness temperature using parameters extracted from the fits to the spectral autocovariance, without imposing any external constraints (e.g. from the fits to the refractive power spectrum).

Fits to the frequency autocovariance functions are shown in Fig. 9. Both models provide close fits to the data, with reduced χ^2 values less than unity. Fit parameters and confidence limits for both thin-screen and extended medium models are listed in Table 2. We note that strong RFI causes difficulties in the spectral normalisation of the 12 Apr. 2004 dataset, which introduces systematic errors in the frequency autocovariance function and the scintillation parameters derived from it. The scintillation and source parameters derived from this dataset should be treated with caution.

In the thin screen model we fit for the products $\Delta\nu_{\rm t} S_{\rm diff}$ and $S_{\rm diff}^{-1}\theta_0/\theta_{\rm cr}$, leaving the flux density of the scintillating component as a free parameter. In the extended medium model we fit to the combination $S_{\rm diff}^2\theta_{\rm cr}^2/\theta_0^2$ because there is a strong degeneracy between between $S_{\rm diff}$ and $\theta_0/\theta_{\rm cr}$ once the source size exceeds $\theta_{\rm cr}$.

Equations (3) and (6) or (7) and (10) are used in conjunction with the fit parameters and scintillation velocity and timescale to derive the screen distance, source size and brightness temperature for either thin- or thick-screen models. These derived source parameters are listed in Table 3.

Many of the quantities derived in Table 3 depend on the scintillation timescale. The scintillation timescale at each epoch is determined by computing the intensity autocovariance function for each 17.5 MHz band and measuring the point at which this falls to $1/e$ of its maximum value. The mean timescale at each epoch is computed by averaging the timescales derived for the various bands. The scintillation timescales are 67 ± 3 min, 40 ± 2 min and 87 ± 3 for 22 Feb. 2004, 12 Apr. 2004 and 30 Jan. 2005 respectively. The quoted error in the timescale is the standard error of the mean, computed from the variation in timescale observed between bands. The band-averaged temporal autocovariance functions for these dates are shown in Fig. 8. In Table 3 the scintillation timescale is expressed as a multiple of 1 h.

We reject the extended medium model because its estimates of the scattering medium properties are unphysical. The large medium depth indicated by this model would place most of the scattering medium well outside the Galactic plane. Formally, the estimated depth is large because, for an extended source scintillating in an extended medium, the diffractive pattern scale s_0 asymptotes to twice the diffractive scale length $r_{\rm diff}$. This fixes the diffractive scale length to a much larger value relative to the thin screen model, in which the pattern scale increases with source size without bound. Thus, in the extended medium model, one requires a large medium depth for a given decorrelation bandwidth since the latter is proportional to $r_{\rm diff}^2/z$. It should be noted that just such a misestimate is

Table 3. Source parameters derived from the best-fit parameters of the various scintillation models applied to the 25 Jan. 2004, 12 Apr. 2004 and 30 Jan. 2005 observations. A range of parameters are permitted by the thin screen model because the diffractively scintillating flux density is unknown. A larger flux density implies a greater source size and lower brightness temperature. The maximum possible flux density is the intrinsic flux density of the entire source, which is approximately 150 mJy. The numbers in the three last columns should be multiplied by the scaling parameter to derive the correct value of each quantity. Here $S_{\rm diff}$ is measured in Jansky, $t_{1\rm h}$ is the diffractive scintillation timescale in hours and v_{50} is the scintillation speed normalised to 50 km s^{-1}.

Model	Quantity	Scaling	25 Jan. 2004	12 Apr. 2004	30 Jan. 2005
Thin screen	Screen distance (pc)	$S_{\rm diff}^{-1} t_{1\rm h}^2 v_{50}^2$	6.0	5.5	6.9
	Source size (μas) ($S_{\rm diff} = 0.05$ Jy)	$t_{1\rm h}^{-1} v_{50}^{-1}$	4.4	4.8	3.8
	Source size (μas) ($S_{\rm diff} = 0.15$ Jy)	$t_{1\rm h}^{-1} v_{50}^{-1}$	15	16	13
	Brightness temperature (K)($S_{\rm diff} = 0.05$ Jy)	$t_{1\rm h}^2 v_{50}^2$	9.1×10^{14}	7.6×10^{14}	12×10^{14}
	Brightness temperature (K)($S_{\rm diff} = 0.15$ Jy)	$t_{1\rm h}^2 v_{50}^2$	2.4×10^{14}	1.9×10^{14}	3.1×10^{14}
Extended medium	Medium thickness (kpc)	$t_{1h}^2 v_{50}^2$	5.7	7.2	5.7
	Source size (μas)	$S_{\rm diff}\, t_{1\rm h}^{-1} v_{50}^{-1}$	3.9	3.1	3.6
	Brightness temperature (K)	$S_{\rm diff}^{-1} t_{1\rm h}^2 v_{50}^2$	1.5×10^{16}	2.4×10^{16}	1.7×10^{16}

expected to occur when the source is extended but is in fact subject to scattering through a thin screen.

We regard the range of the brightness temperatures derived at different epochs as the most faithful estimate of their true uncertainty. Part of the range can be attributed to the uncertainty in the scattering speed and scintillation timescale, both of which change between epochs. The minimum brightness temperature is uncertain by a factor of two even when reasonable variations in these parameters are taken into account and the RFI-afflicted 12 Apr. 2004 dataset is excluded. The uncertainty may reflect other uncertainties not taken into account by the model, such as anisotropy in the source and scattering medium.

We note that the nearby pulsar PSR 1813+4013 is observed to exhibit a diffractive decorrelation bandwidth of ∼10 MHz at 1.4 GHz (B. Stappers, private communication). If the scattering properties of J1819+3845 are comparable then this decorrelation bandwidth favours a value of $S_{\rm diff}$ around 100 mJy, and a brightness temperature toward the low end of its allowed range.

3.3.3. Source spectral changes

In the scintillation model above the brightness temperature depends on the free parameter $S_{\rm diff}$. We discuss here the extent to which the spectrum of the component undergoing scintillation matches the mean source spectrum, and whether this component makes a significant contribution to the overall intrinsic source spectrum at low frequencies. The latter might be expected if the source is comprised of multiple components with distinct spectra. Evidence that this may be case comes from analysis of the 4.9 and 8.4 GHz light curves, in which distinctly different polarization and total intensity fluctuations imply that the source is composed of at least two bright features (Macquart et al. 2003).

Despite the source's complex structure, its mean spectrum between 1.4 and 8.4 GHz is a power law with a spectral index of 0.8. We have also measured the spectral index of the source from the variation in mean flux density across the band from our 21 cm observations. These measured spectral indices, listed in Table 4, varying between 0.8 and 1.2, are, with one significant exception, *consistent* with the intrinsic spectral index derived on the basis of long-term measurements between 1.4 and 8.4 GHz (de Bruyn et al., in prep.). It is difficult to be more precise, since our 1.4 GHz spectral measurements are a poor indicator of the intrinsic source spectrum when only a few diffractive scintles are observed, as is the case in many of our observations.

The one notable exception is the spectrum measured on 22 Feb. 2003, which is wildly at variance with the mean source spectrum and with the other observations. This difference may be significant, because the average spectrum extracted from this observation encompasses many diffractive scintles. This difference may reflect the emergence of a new component in the source. However, no discernible deviation in the amplitude of diffractive scintillation is associated with this epoch.

4. Discussion

4.1. Robustness of the brightness temperature estimate

The $\gtrsim 10^{14}$ K brightness temperature implied by the diffractive scintillation properties of J1819+3845 is difficult to account for using the standard interpretation of AGN radio emission in terms of synchrotron emission. In this section we consider the robustness of this estimate.

The greatest source of error in the thin-screen model is associated with the effect of anisotropy on the scale of the scintillation pattern, s_0, which propagates into the estimation of $r_{\rm diff}$. Scattering measurements of pulsars (Mutel & Lestrade 1990; Spangler & Cordes 1998) suggest that the maximum degree of anisotropy expected due to turbulence in the interstellar medium is 3:1. However, intensity variations in the regime of weak scattering at 4.9 GHz indicate that the scintillation pattern of J1819+3845 has an axial ratio of $14^{+>30}_{-8}$ (Dennett-Thorpe & de Bruyn 2003). The relative contributions of medium and source to this overall anisotropy are unknown at this frequency. At 1.4 GHz the source structure is expected to be the primary

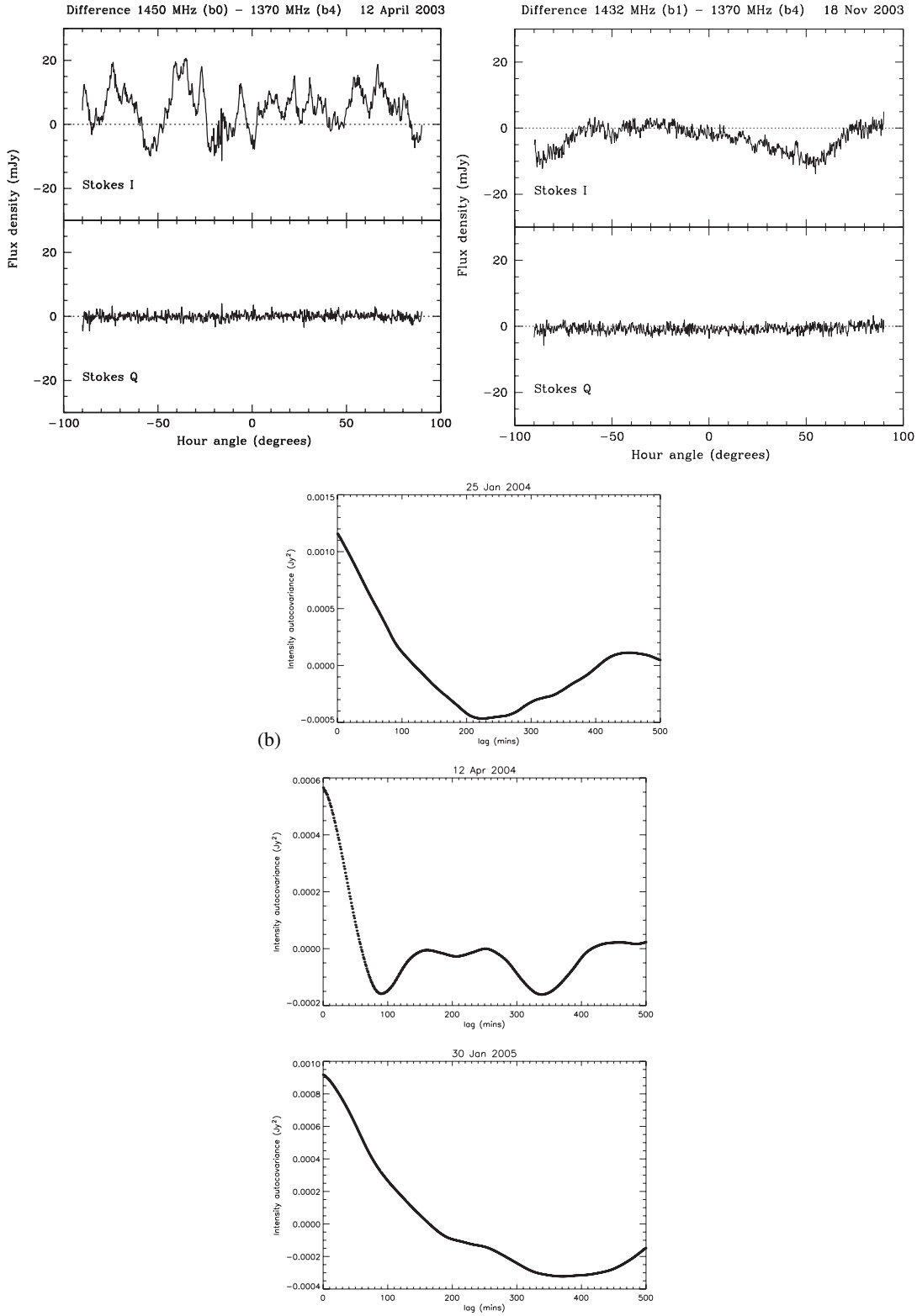

Fig. 8. a) Two sample difference light curves, from 12 Apr. 2003 (fast season) and 18 Nov. 2003 (slow season). The rapid, sharp variations of these frequency-dependent intensity fluctuations, particularly on 12 Apr. 2003, are well above the 1.4 mJy noise level. Note that the rapid frequency-dependent fluctuations are absent in the slow season. **b)** Autocovariance functions of the temporal intensity fluctuations on 25 Jan. 2004, 12 Apr. 2004, 30 Jan. 2005. Note that the amplitude of the function at zero temporal lag significantly exceeds the amplitude observed in the spectral autocovariance function (see Fig. 9). The excess can be attributed to the additional influence of refractive scintillation on the temporal modulations.

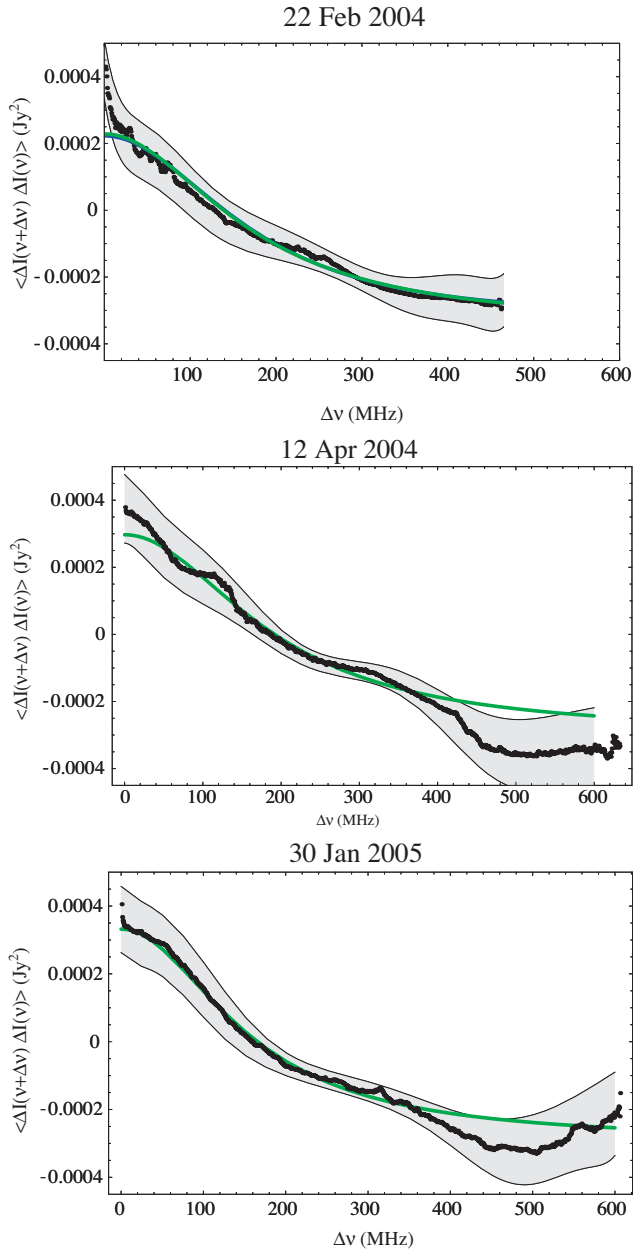

Fig. 9. Fits to the spectral decorrelation characteristics of the diffractive scintillation. The grey error regions incorporate both uncertainties due to the finite number of diffractive scintles incorporated in the fit and uncertainties in the mean spectrum of the diffractively scintillating component. The green and blue lines represent, respectively, the best fitting spectral decorrelation functions expected from a thin phase changing screen and from an extended scattering medium. Where only one line is visibile the fits are identical. The plots shown here are the averages of the autocorrelations from ≈ 720 time slots for each observation. The observed decorrelation bandwidths (half-width at half maximum) are 170, 192 and 156 MHz for the three epochs respectively. (This figure is available in colour in electronic form.)

agent responsible for any anisotropy in the scintillation pattern because the source substantially exceeds the critical angular scale of the diffraction pattern. We estimate $3.2 < \theta_0/\theta_{\rm cr} < 37$ for $50 < S_{\rm diff} < 150$ mJy (see Table 2).

Table 4. The variation in mean flux density and spectral index of J1819+3845 with observing date. Here the spectral index α, defined as $S \propto \nu^{\alpha}$, is derived solely on the basis of the spectrum exhibited across the band at 1.4 GHz. Blanks and bracketed values indicate observations in which so few diffractive scintles are present that the mean spectrum is a poor representation of the mean source spectrum, and blanks indicate instances for which a power law is an unacceptable fit to the mean spectrum. The errors quoted in the spectral index reflect only formal errors associated with a fit to a power law.

Date	Mean flux density (mJy)	Spectral index α
14 Jun. 2002	85	0.79 ± 0.01
30 Aug. 2002	80	–
22 Feb. 2003	144	0.29 ± 0.01
12 Apr. 2003	111	1.01 ± 0.01
19 Jun. 2003	115	1.19 ± 0.01
22 Aug. 2003	242	(1.21 ± 0.02)
18 Nov. 2003	151	–
25 Dec. 2003	147	1.05 ± 0.01
22 Feb. 2004	144 (at 1.40 GHz)	0.90 ± 0.06
12 Apr. 2004	143 (at 1.40 GHz)	0.67 ± 0.02
30 Jan. 2005	167 (at 1.40 GHz)	0.50 ± 0.03

Anisotropy in the source must couple with anisotropy intrinsic to the turbulence in the scattering medium to cause an appreciable misestimate of the source size. This is because any source elongation oriented parallel to the medium anisotropy would not be detected by a reduction in the scintillation amplitude. In this case an anisotropic ratio of ζ would lead to a misestimate of the source size by a factor of ζ along one source axis and a brightness temperature misestimate of a factor of ζ. Anisotropy in the source alone is insufficient to cause a serious misestimate of its brightness temperature, because the source extension would manifest itself through a reduction in the modulation amplitude of the scintillation; although the source is assumed to be circularly symmetric in our fits above, the reduction of the modulation amplitude would lead us to deduce a source angular size somewhere between the lengths of the short and long axes of the source.

We have performed an analysis of the variation in scintillation time scale at 21 cm. An annual cycle in the timescale is clearly observed, but anisotropy in the scintillation pattern is not required to reproduce the timescale variations observed from our observations to date. Changes in the magnitude of the scintillation velocity, as the Earth's velocity changes with respect to the scattering medium's, are alone sufficient to reproduce the annual cycle.

Another shortcoming of the scattering models resides in the assumption that the scattering occurs in the regime of asymptotically strong scintillation. The scattering strength $r_{\rm F}/r_{\rm diff}$ is derived from the decorrelation bandwidth. The decorrelation bandwidth in the thin-screen model is at most $\Delta\nu_{\rm t}$ = 78 MHz for $S_{\rm diff}$ = 50 mJy, which implies a scattering strength ≈4.2. For $S_{\rm diff}$ = 150 mJy the decorrelation bandwidth is 26 MHz, implying a scattering strength of 7. The scintillation is sufficiently strong to be applicable to the present situation.

Certainly, any errors introduced by this approximation are minor relative to those introduced by possible anisotropy in the scintillation pattern.

4.2. Relationship to 6 cm source structure and scattering properties

It is important to consider how the structure of the source derived here relates to that inferred on the basis of the weak scintillation exhibited by the source at 4.9 GHz.

The source angular size derived at 1.4 GHz for any given screen distance (cf. Sect. 3.3.1) is approximately three times smaller than that inferred at 4.9 GHz. This would seem surprising because one would expect that the source, whose spectrum does not fall off as fast as that of a uniform synchrotron self-absorbed source ($\alpha = +2.5$) should be substantially larger at 1.4 GHz. A straightforward comparison between the scintillation properties at 1.4 GHz and 4.9 GHz is complicated by these opacity effects. Significant parts of the source that are visible at 4.9 GHz, and contribute to the observed scintillations, may well be hidden at 1.4 GHz. On the other hand, the diffractively scintillating component need only comprise a small fraction of the total source emission at 6 cm because weak and diffractive scintillation are sensitive to structure on widely different angular scales. Weak scintillation responds to all structure on angular scales $\lesssim\theta_{\rm F}$ whereas diffractive scintillation produces a strongly identifiable response specifically to structure on much smaller angular scales, $\sim\theta_{\rm cr}$. Thus the small structure responsible for the diffractive scintillation at 1.4 GHz may well be present at 4.9 GHz but the signature of its presence could be masked by the dramatic variations due to the rest of the source. It is also possible that the source has multiple components at both 1.4 GHz and 4.9 GHz with very different spectral indices. For example, a coherent emitter (see the next section) could well have a very steep spectrum which would contribute a negligible fraction of the emission at 4.9 GHz.

Recent observations suggest that this may indeed be the case. We may have detected evidence for the component responsible for diffractive scintillation in the weak scattering of the source at 4.9 GHz. Observations from Dec. 2003 to Apr. 2004 at 4.9 GHz indicate the emergence of 5–10 mJy variations on a timescale of <15 min superposed on the ~200 mJy peak-to-peak, ≈40 min variations normally observed at 4.9 GHz at this time of year. It is possible that the scintillation at 1.4 GHz, which is more sensitive to fine structure, first detected the same feature which was subsequently detected at higher frequencies. We continue to monitor the source and will return to this apparent evolution in the future.

The screen distance indicated by the model in Sect. 3.3.2 is larger than the 4−12 pc value estimated by Dennett-Thorpe & de Bruyn (2003) assuming isotropic turbulence to model the intensity fluctuations observed in the regime of weak scattering at 4.9 GHz. The minimum distance implied by the present thin-screen model is $\sim 40\, t_{1hr}^2 v_{50}^2$ pc if $S_{\rm diff} = 150$ mJy. An obvious reason for this discrepancy is that anisotropy is not taken into account in the estimate of the screen distance at 4.9 GHz, and we have no detection of anisotropy at 1.4 GHz.

4.3. Problems with high brightness temperature emission

The high brightness temperature exhibited by a component of J1819+3845 raises concerns regarding the interpretation of AGN emission in terms of incoherent synchrotron radiation. Inverse Compton scattering limits the brightness temperature of incoherent synchrotron emission to 10^{12} K (Kellerman & Pauliny-Toth 1969) but equipartition arguments (Readhead 1994) suggest that the actual limit should be an order of magnitude below this. Bulk motion with a Doppler boosting factor $\delta \gtrsim 100$ is required to reconcile the observed brightness temperature with its maximum possible rest-frame value. Such high bulk motions are problematic because they imply unacceptably high jet kinetic energies. Synchrotron emission is also extremely radiatively inefficient in this regime, and it is questionable whether $\Gamma \gtrsim 100$ motions are compatible with the hypothesis of incoherent synchrotron radiation (Begelman et al. 1994).

In view of the difficulties confronted by an explanation involving synchrotron radiation, it is appropriate to consider whether a coherent emission mechanism provides a more acceptable explanation of the high brightness temperature. The nature of coherent emission requires the source to be composed of a large number of independently radiating coherent "bunches", with individual brightness temperatures far in excess of the $T_{\rm b} \gtrsim 10^{14}$ K value derived here (e.g. Melrose 1991). This is because the coherence volume of any one coherent bunch is microscopic compared to the light-week dimensions of the source. Further, the short lifetime associated with any individual coherent bunch would require emission from a large number of independent subsources to explain the constancy of the emission observed on 12-h to 6-monthly timescales.

Coherent emission from each bunch is expected to be highly polarized. The upper limit of 1% overall source polarization at 1.4 GHz limits the polarization associated with the diffractive component from ≈1%, for $S_{\rm diff} = 150$ mJy, to 3%, for $S_{\rm diff} = 50$ mJy. This suggests that either the emission is efficiently depolarized as it escapes the source or that the emission is intrinsically unpolarized. The latter would occur if the magnetic field is highly disordered within the emission region, so that the polarizations of individual coherent patches would be diluted when averaged over the entire region.

Another important obstacle relates to the escape of extremely bright emission from the source region. Induced Compton scattering places an extremely stringent limit on the thermal electron density of the source: for a path length L the electron density must satisfy

$$n_{\rm e} \ll \frac{1}{\sigma_T L}\left(\frac{T_{\rm b}}{5\times10^9\,{\rm K}}\right)^{-1} = 2.4\left(\frac{L}{1\,{\rm pc}}\right)^{-1}\left(\frac{T_{\rm b}}{10^{15}\,{\rm K}}\right)^{-1}\ {\rm cm}^{-3}, \quad (13)$$

for induced Compton scattering to be unimportant. It is argued that this density is incompatible with the high densities required to efficiently generate coherent emission in the first place (e.g. Coppi et al. 1993). This difficulty may be overcome by appealing to a highly anisotropic photon distribution. However, this explanation is also problematic because such highly beamed emission acts like a particle beam

in exciting Langmuir waves which also scatter the radiation (Gedalin & Eichler 1993; Luo & Melrose 1995). This effect is the accepted mechanism for the occultation of several eclipsing radio pulsars whose radiation propagates through a relatively low density stellar wind. Applied in the context of AGN, this effect would require unreasonably low electron densities in the emission and ambient media to permit the escape of coherent emission from the source (Levinson & Blandford 1995).

Begelman et al. (2005) have recently proposed an electron-cyclotron maser model for the high brightness temperature emission inferred in some IDV sources. They discuss in much more detail the difficulties associated with the escape of bright radiation from a source. They conclude that it is possible for the high brightness radiation observed in J1819+3845 to escape, subject to certain constraints on the location of the emission region.

5. Conclusions

We have detected the diffractive interstellar scintillation from the quasar J1819+3845 at 1.4 GHz. This detection is notable because it constitutes the first detection of this phenomenon in an AGN, and it implies that a component of the source must be extremely compact.

These scintillations are analysed in the context of thin-screen and extended-medium models for the distribution of interstellar scattering material. The timescale, bandwidth and amplitude of the variations at 21 cm imply a brightness temperature $\gtrsim 10^{14}$ K.

Acknowledgements. The WSRT is operated by The Netherlands Foundation for Research in Astronomy (NFRA/ASTRON) with financial support by the Netherlands Organization for Scientific Research (NWO). We thank Ben Stappers, Barney Rickett and Bill Coles for discussions and useful comments.

References

Baars, J. W. M., Genzel, R., Pauliny-Toth, I. I. K., & Witzel, A. 1977, A&A, 61, 99
Begelman, M. C., Rees, M. J., & Sikora, M. 1994, ApJ, 429, L57
Begelman, M. C., Ergun, R. E., & Rees, M. J. 2005, ApJ, 625, 51
Bignall, H. E., Jauncey, D. L., Lovell, J. E. J., et al. 2003, ApJ, 585, 653
Chashei, I. V., & Shishov, V. I. 1976, Soviet Astron., 20, 13
Coles, W. A., Frehlich, R. G., Rickett, B. J., & Codona, J. L. 1987, ApJ, 315, 666
Codona, J. L., & Frehlich, R. G. 1987, Radio Science, 22, 469
Condon, J. J., & Backer, D. C. 1975, ApJ, 197, 31
Coppi, P., Blandford, R. D., & Rees, M. J. 1993, MNRAS, 262, 603
Dennett-Thorpe, J., & de Bruyn, A. G. 2000, ApJ, 529, L65
Dennett-Thorpe, J., & de Bruyn, A. G. 2002, Nature, 415, 57
Dennett-Thorpe, J., & de Bruyn, A. G. 2003, A&A, 404, 113
Dennison, B., & Condon, J. J. 1981, ApJ, 246, 91
Ewing, M. S., Batchelor, R. A., Friefeld, R. D., Price, R. M., & Staelin, D. H. 1970, ApJ, 162, L169
Gedalin, M., & Eichler, D. 1993, ApJ, 406, 629
Goodman, J., & Narayan, R. 1985, MNRAS, 214, 519
Gwinn, C. R., Britton, M. C., Reynolds, J. E., et al. 1998, ApJ, 505, 928
Heeschen, D. S. 1984, AJ, 89, 1111
Jauncey, D. L., & Macquart, J.-P. 2001, A&A, 370, L9
Jauncey, D. L., Kedziora-Chudczer, L. L., Lovell, J. E. J., et al. 2000, in Astrophysical Phenomena Revealed by Space VLBI, Insitute of Space and Astronautical Science, 147
Jenkins, G. M., & Watts, D. G. 1968, Spectral Analysis and its Applications, Holden-Day
Kedziora-Chudczer, L., Jauncey, D. L., Wieringa, M. H., et al. 1997, ApJ, 490, L9
Kellerman, K. I., & Pauliny-Toth, I. I. K. 1969, ApJ, 155, L71
Levinson, A., & Blandford, R. 1995, MNRAS, 274, 717
Lovell, J. E. J., Jauncey, D. L., Bignall, H. E., et al. 2003, AJ, 126, 1699
Luo, Q., & Melrose, D. B. 1995, ApJ, 452, 346
Macquart, J.-P., de Bruyn, A. G., & Dennett-Thorpe, J. 2002, in Active Galactic Nuclei: from Central Engine to Host Galaxy, ASP Conf. Ser., 290, 349
Macquart, J.-P., Kedziora-Chudczer, L., Rayner, D. P., & Jauncey, D. L. 2000, ApJ, 538, 623
Melrose, D. B. 1991, ARA&A, 29, 31
Mutel, R. L., & Lestrade, J.-F. 1990, ApJ, 349, L47
Narayan, R. 1992, Phil. Trans. R. Soc. Lond. A, 341, 151
Papoulis, A. 1991, Probability, random variables, and stochastic processes, 3rd ed. (New York: McGraw Hill)
Quirrenbach, A., Witzel, A., Wagner, S., et al. 1991, ApJ, 372, L71
Quirrenbach, A., Kraus, A., Witzel, A., et al. 2000, A&AS, 141, 221
Readhead, A. C. S. 1994, ApJ, 426, 51
Rickett, B. J. 1970, MNRAS, 150, 67
Rickett, B. J., Witzel, A., Kraus, A., Krichbaum, T. P., & Qian, S. J. 2001, ApJ, 550, L11
Rickett, B. J., Kedziora-Chudczer, L., & Jauncey, D. L. 2002, ApJ, 581, 103
Spangler, S. R., & Cordes, J. M. 1998, ApJ, 505, 766
Witzel, A., Heeschen, D. S., Schalinski, C., Krichbaum, Th. 1986, Mit.A.G., 65, 239

Online Material

Appendix A: Determination of errors in the spectral autocorrelation function

The finite number of scintles measured during each observation must be taken into account when comparing the spectral autocovariance curves shown in Fig. 9 to the theoretical models, which represent an average over the ensemble of all possible scintles.

The deviation in the sample autocovariance function from the ensemble-average autocovariance can be characterised in terms of the the variance in the sample autocovariance function, $C(\tau)$, given by (Jenkins & Watts 1968, Eq. (5.3.21))

$$\mathrm{var}[C(\tau)] = \frac{1}{(T-|\tau|)^2}\int_{-(T-\tau)}^{T-\tau}(T-\tau-r)[\gamma(r)^2 - \gamma(r+\tau)\gamma(r-\tau)]\,\mathrm{d}r, \quad \text{(A.1)}$$

where T is the length of the sample dataset and $\gamma(\tau)$ is the ensemble-average autocovariance.

We wish to determine the error in the spectral autocovariance of a single time slot. The ensemble average spectral autocovariance is unknown but, in order to determine the error in C_ν, we approximate its form using the best-fitting thin screen autocovariance function. The error for a single time channel is determined by numerically integrating this model in Eq. (A.1), with T set to the total bandwidth spanned during the observation.

The final spectral autocorrelations shown in Fig. 9 represent an averages over many diffractive scintles observed during a 12-h duration. We assume that the autocovariance estimates of the individual diffractive scintles are statistically independent, so that the errors deduced from Eq. (A.1) are reduced by the square root of the number of diffractive scintles contributing to C_ν. This is estimated by comparing the observing duration to the diffractive timescale.

These sampling errors are combined linearly with spectral misestimation errors (see Sect. 3.2) to derive the error regions depicted in Fig. 9. Sampling errors dominate at all spectral lags.